

Communication

Yolk-Shell Nanocrystal@ZIF-8 Nanostructures for Gas Phase Heterogeneous Catalysis with Selectivity Control

Chun-Hong Kuo, Yang Tang, Lien-Yang Chou, Brian T Sneed, Casey N Brodsky, Zipeng Zhao, Chia-Kuang (Frank) Tsung, and Lien-Yang Chou

J. Am. Chem. Soc., **Just Accepted Manuscript** • DOI: 10.1021/ja306869j • Publication Date (Web): 17 Aug 2012

Downloaded from <http://pubs.acs.org> on August 19, 2012

Just Accepted

“Just Accepted” manuscripts have been peer-reviewed and accepted for publication. They are posted online prior to technical editing, formatting for publication and author proofing. The American Chemical Society provides “Just Accepted” as a free service to the research community to expedite the dissemination of scientific material as soon as possible after acceptance. “Just Accepted” manuscripts appear in full in PDF format accompanied by an HTML abstract. “Just Accepted” manuscripts have been fully peer reviewed, but should not be considered the official version of record. They are accessible to all readers and citable by the Digital Object Identifier (DOI®). “Just Accepted” is an optional service offered to authors. Therefore, the “Just Accepted” Web site may not include all articles that will be published in the journal. After a manuscript is technically edited and formatted, it will be removed from the “Just Accepted” Web site and published as an ASAP article. Note that technical editing may introduce minor changes to the manuscript text and/or graphics which could affect content, and all legal disclaimers and ethical guidelines that apply to the journal pertain. ACS cannot be held responsible for errors or consequences arising from the use of information contained in these “Just Accepted” manuscripts.



Yolk-Shell Nanocrystal@ZIF-8 Nanostructures for Gas Phase Heterogeneous Catalysis with Selectivity Control

Chun-Hong Kuo, Yang Tang, Lien-Yang Chou, Brian T. Sneed, Casey N. Brodsky, Zipeng Zhao, and Chia-Kuang Tsung*

Department of Chemistry, Merkert Chemistry Center, Boston College, 2609 Beacon Street, Chestnut Hill, Massachusetts 02467, United States.

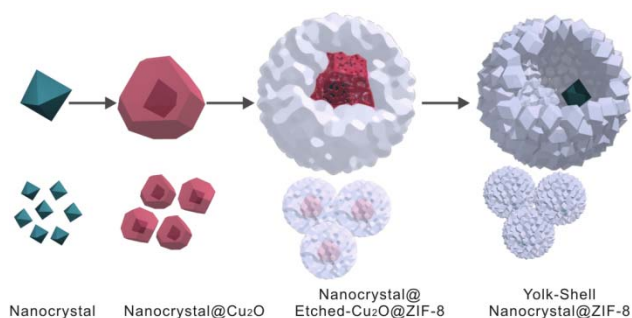
Supporting Information Placeholder

ABSTRACT: A general synthetic strategy for yolk-shell nanocrystal@ZIF-8 nanostructures is developed. The yolk-shell nanostructures possess the functions of nanoparticle cores, microporous shells, and a cavity in-between, which offer great potential in heterogeneous catalysis. The synthetic strategy involved first coating the nanocrystal cores with a layer of Cu_2O as the sacrificial template and then a layer of polycrystalline ZIF-8. The clean Cu_2O surface assists the ZIF-8 layer coating and is etched off spontaneously and simultaneously during the ZIF-8 coating. The yolk-shell nanostructures were characterized by TEM, SEM, XRD and nitrogen adsorption. To study the catalytic behavior, model reactions including ethylene, cyclohexene, and cyclooctene hydrogenations were carried out over the Pd@ZIF-8 catalysts. The microporous ZIF-8 shells provide excellent molecular-size selectivity. The results show high activity in ethylene and cyclohexene hydrogenations but not in cyclooctene hydrogenation. Different activation energies for cyclohexene hydrogenation were obtained for the nanostructures with and without the cavity in-between the core and shell. This demonstrates the importance of controlling the cavity because of its influence on the catalysis.

Yolk-shell nanostructures have caused a recent interest in research for their potential in heterogeneous catalysis¹, photocatalysis², and biomedicine applications.^{3,4} Integrating the functions of the nanocrystal core, nanostructured shell, and the cavity in-between provides a tool to optimize the performance of a nanomaterial. In the yolk-shell catalysts, the metal core provides a catalytically active surface for the reactions and the porous shell serves as a barrier layer to prevent aggregation of the active surface with neighboring metal cores during the reactions. Compared to core-shell nanostructures,⁵ in which the shell is directly on the metal surface, the cavity between the core and shell in the yolk-shell structures not only reserves a larger exposed metal surface for the reactants but also makes the reactants interact with the surface more homogeneously. It has been proposed that the shells in the yolk-shell structures could introduce multiple functions into the catalysts such as regulation of diffusion and control of molecular size-selectivity; however,

in most of the previous yolk-shell catalysts, the shell only serves one function, a protective layer to prevent aggregation between particles during the reactions.⁶⁻¹³ This is mainly because in previous works, the shell materials were limited to non-ordered porous materials, which restricts the functions of the shells. Here, we report a general method for the synthesis of yolk-shell structures with metal organic framework (MOF) shells. The uniform and controllable microporous structure, large internal surface area, and tunable chemical property of the MOF shell could introduce new functions into the yolk-shell nanostructures and make the yolk-shell structures more attractive to different applications. We chose zeolitic imidazolate frameworks-8 (ZIF-8) as the shell material to demonstrate our method. ZIF-8, a subclass of MOFs, is of high thermal and chemical stability.¹⁴ It is one of the few commercially available MOFs because of its great potential in gas separation¹⁵⁻¹⁷ and gas storage.^{18,19}

Scheme 1. The growth procedure of the nanocrystal@ZIF-8 yolk-shell nanostructures.



Most of the previously reported synthetic strategies of incorporating nanocrystals into MOFs used gas-phase infiltration or grinding, such as Au@ZIF-8^{20,21} and Cu/ZnO@MOF-5²². These post-incorporating methods cannot create the cavity around the nanocrystal core and the morphology of the nanocrystal cores is uncontrollable. The morphology is a very important factor in the function of nanocrystals for catalytic and optical properties. Furthermore, in these post-incorporating methods, the porous structures of MOF could be damaged during the incorporation and some of the nanocrystals were on the external surface of MOFs. A preferred

strategy, coating MOFs on the preformed nanocrystals, was reported recently but the synthesis of MOF yolk-shell nanostructures is still challenging.²³ In this work, we develop a new strategy. Scheme 1 illustrates the synthetic strategy. Metal nanocrystals were first coated with a layer of a sacrificial template and then coated with ZIF-8. We specifically choose Cu_2O as the sacrificial template. Not only could the Cu_2O be etched simultaneously and spontaneously by the protons generated during the formation of ZIF-8 but also the capping agent free surface of Cu_2O provides a clean surface for ZIF-8 coating. Also, methods of Cu_2O coating on different nanocrystals have been well-developed, which makes our synthetic strategy general and versatile.²⁴

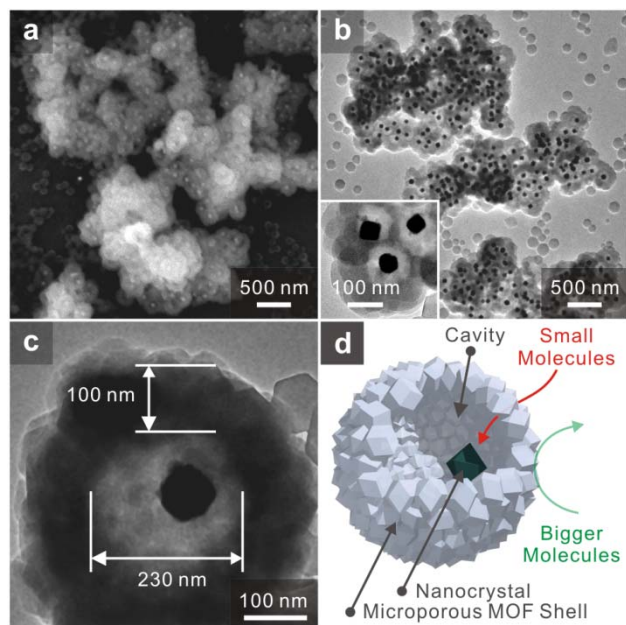


Figure 1. The nanocrystal@ZIF-8 yolk-shell nanostructure. (a) The scanning electron micrograph (SEM). (b) and (c) The transition electron micrograph (TEM). The cores are Pd octahedrons with edge sizes of 60 nm and the shells are microporous ZIF-8 with thickness of around 100 nm. (d) A schematic sketch of the yolk-shell nanostructure.

A typical single shape-controlled metal nanocrystal incorporated in crack-free polycrystalline ZIF-8 crystals is shown in Figure 1 and Figure S1. The shape and size of nanocrystals were well maintained during the synthesis. All the nanocrystals were incorporated in ZIF-8. A small amount of ZIF-8 crystals with no nanocrystals were also formed, which could be removed by centrifugation. In order to demonstrate that we can preserve the size and shape of the nanocrystals by using this strategy, relatively large shape controlled metal nanocrystals were used. The same method could be applied to differently sized nanocrystals. In a typical synthesis, Pd octahedrons²⁵ were coated by Cu_2O to form a Pd@ Cu_2O core-shell structure (Figure S2a). After Cu_2O coating, the Pd@ Cu_2O structure was mixed with ZIF-8 precursors, 2-methylimidazole (2-melm) and zinc nitrate in methanol.²⁶ As the pH of the solution decreased from 7 to 5 during the formation of ZIF-8 because of the de-protonation of 2-melm during the formation of ZIF-8, the Cu_2O was etched off simultaneously.¹⁰ A trace amount of the Cu_2O residue was observed (Figure S2b). A solution of 3% NH_4OH in methanol was used to remove the trace amount of residual Cu_2O in the

final step. The products were then washed with methanol and collected by centrifugation. The absence of the Cu signal in the element analysis (ICP-AES) confirms the removal of Cu_2O in the final products. The SEM and TEM images (Figure 1) show that the Pd nanocrystals are well-separated by the ZIF-8 shells. The inset of Figure 1 clearly shows the well-preserved morphology of the nanocrystals after the coating as well as the cavity. The thickness of the ZIF-8 is around 100 nm and the ZIF-8 is polycrystalline and crack-free, which is further confirmed by the catalysis results later. The solution colors of these samples at different stages are shown in Figure S3. After the Pd nanocrystals were coated with Cu_2O , the color changed from brown to green which indicates the formation of Cu_2O shells.²⁴ During the ZIF-8 coating, the color gradually turned back to brown but was turbid, which indicates the depletion of Cu_2O and the simultaneous formation of ZIF-8.

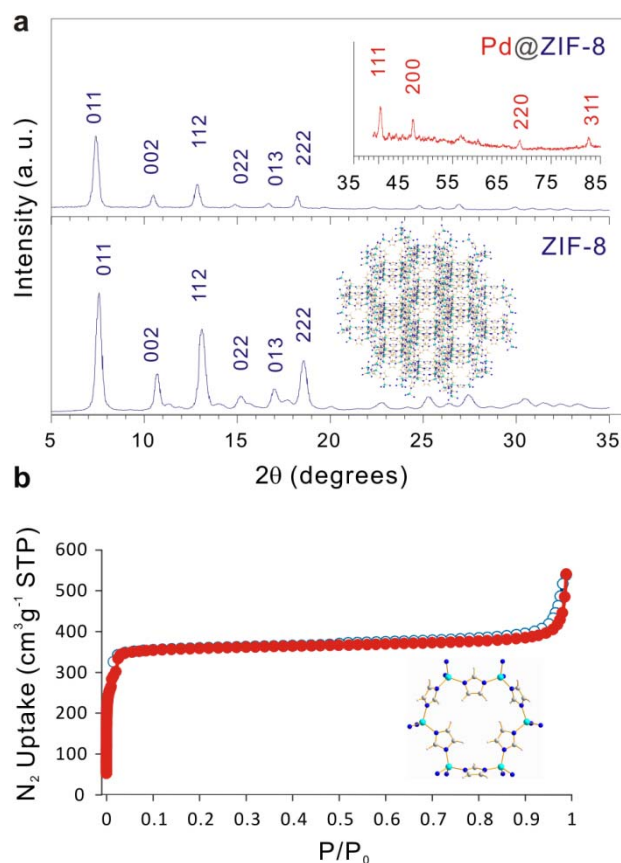


Figure 2. The crystal and pore structures of Pd@ZIF-8 yolk-shell nanostructure. (a) Powder X-ray diffraction patterns of the yolk-shell nanostructure and pure ZIF-8 crystals. The peaks of the ZIF-8 shells (upper) correspond to those of the pure ZIF-8 nanocrystals, which reveals that the ZIF-8 shells have the same crystal structure as the pure ZIF-8 crystals. The inset shows the higher angle diffraction peaks contributed by the Pd octahedrons. (b) Nitrogen adsorption-desorption isotherm of the Pd@ZIF-8 yolk-shell nanostructure shows the type-I behavior and confirms the microporous structure of the ZIF-8 shells. The BET surface area is 1396 m^2/g .

The crystal structure and porosity of the shell were studied by powder X-ray diffraction (XRD) and nitrogen-sorption

measurements. The XRD patterns of pure ZIF-8 and Pd@ZIF-8 yolk-shell nanostructure are shown in Figure 2a. Both patterns generated from the ordered porous structure of ZIF-8 shells (2θ , 5° - 35°)²⁷ and the Pd cores (2θ , 35° - 85°) were observed for Pd@ZIF-8 yolk-shell nanostructure. All the prominent peaks of the ZIF-8 shells, including 011, 002, 112, 022, 013, and 222, correspond to those of pure ZIF-8 crystals. This confirms the sodalite zeolite-type crystal structure of the ZIF-8 shell and the well-defined peaks reveal the high crystallinity. The nitrogen adsorption-desorption isotherm (Figure 2b) of the Pd@ZIF-8 yolk-shell nanostructure displays type-I behavior. The steep step at low relative pressure reveals that the shells are microporous. The specific surface area estimated by the BET method is 1396 m²/g. The lower surface area of the yolk-shell structure compared with pure ZIF-8 (1643 m²/g)²³ is mainly due to the heavier and nonporous metal cores. Thermal stability of the yolk-shell structure was characterized by thermogravimetric analysis (Figure S4). The decomposition temperature of Pd@ZIF-8 yolk-shell nanostructure is 425°C which is only marginally lower than that of pure ZIF-8 crystals (470°C). This difference can be contributed by the crystal size difference between the ZIF-8 shells and few hundred nanometer pure ZIF-8 crystals.

Table 1. The catalytic behaviors of different ZIF-8 nanostructures.

| | | Pd@ZIF-8 core-shell | Pd@ZIF-8 yolk-shell | Pd on ZIF-8 |
|--------------------------|--|------------------------|------------------------|----------------------|
| Ethylene ^a | Activity ^b (mol·g _{Pd} ⁻¹ ·s ⁻¹) | 1.3×10 ⁻² | 3.2×10 ⁻³ | 3.0×10 ⁻³ |
| | Ea ^c (kJ/mol) | 41.7 | 42.7 | 41.0 |
| | Activity ^b (mol·g _{Pd} ⁻¹ ·s ⁻¹) | 1.5×10 ⁻⁴ | 3.2×10 ⁻⁵ | 2.8×10 ⁻⁵ |
| Cyclohexene ^a | TOF (s ⁻¹) | 0.27 | 0.23 | 0.21 |
| | Ea ^c (kJ/mol) | 27.5 | 40.1 | 41.1 |
| | Activity ^b (mol·g _{Pd} ⁻¹ ·s ⁻¹) | N/A | N/A | 2.8×10 ⁻⁶ |
| Cyclooctene ^a | TOF (s ⁻¹) | N/A | N/A | 0.02 |
| | Ea ^c (kJ/mol) | N/A | N/A | 34.9 |

^a In each experiment: 10 torr hydrocarbon (C₂H₄, C₆H₄, or C₈H₁₄), 100 torr H₂, and 650 torr He at 323 K.

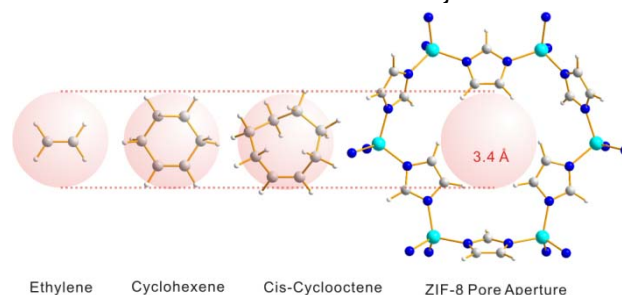
^b The metal loading was determined by elemental analysis and used to normalize the conversion to mass of Pd.

^c Arrhenius activation energy.

Gas-phase hydrogenation of ethylene, cyclohexene, and cyclooctene were carried out to study the molecule size-selective catalysis. (Scheme 2) The catalysts of 60 nm Pd nanocrystal@ZIF-8 yolk-shell nanostructure (yolk-shell Pd@ZIF-8), 60 nm Pd nanocrystals directly deposited on ZIF-8 crystal surfaces (Pd on ZIF-8), and 20 nm Pd nanocrystals coated by ZIF-8 layers without the cavity (core-shell Pd@ZIF-8) were prepared for comparison. Table 1 shows the activities and activation energies of the reactions. For ethylene hydrogenation, all the catalysts show high activity and similar activation energies, which indicates the same ethylene hydro-

genation kinetics. It also shows that there is no significant diffusional influence caused by the ZIF-8 shells. The activity difference is mainly due to the size difference of Pd nanocrystals. Using the same nanocrystals for different catalysts is challenging because the core-shell synthetic strategy is different from the yolk-shell strategy; however, after the normalizing by the Pd surface area, the activities are similar. For the cyclooctene hydrogenation, both the core-shell and yolk-shell catalysts show no detectable activity but the Pd on ZIF-8 catalyst shows good activity. This result clearly exhibits the molecule-size-selective property of the ZIF-8 shells. Ethylene molecules are small (2.5 Å) enough to diffuse through the pore apertures of the ZIF-8 shells (3.4 Å) without serious hindrance; however, the size of the cyclooctene molecules (5.5 Å) are much bigger than the size of the pore aperture. Therefore, only the catalyst in which the Pd nanocrystals were directly deposited on the external surface of ZIF-8 (Pd on ZIF-8) shows activity for cyclooctene hydrogenation. This result also clearly suggests that the ZIF-8 shells of both yolk-shell and core-shell are devoid of cracks or fractures. No significant deactivation was observed even when the catalysts were heated to 150°C. The catalysts were checked after the reactions by TEM. Most of them still maintain the yolk-shell structure.

Scheme 2. Molecule size-selective catalysis.



Cyclohexene hydrogenation displays very interesting catalytic phenomena in this series of hydrogenation reactions. Although the size of cyclohexene molecules (4.2 Å) is comparable to the aperture size of ZIF-8, all the catalysts show good activities for cyclohexene hydrogenation. This indicates the flexibility of ZIF-8 frameworks.²⁸ The yolk-shell Pd@ZIF-8 catalyst and Pd on ZIF-8 have similar activation energies. The core-shell Pd@ZIF-8 catalyst has lower activation energy. To exclude the chance that the activation energy difference is contributed by capping agents or supports, a series of Pd nanocrystals were prepared by using different capping agents, and then were directly deposited on different supports. Table S1 shows the activation energies of all the catalysts. The values of the activation energies are all around 40 kJ/mol; except for the core-shell Pd@ZIF-8 catalyst, which is lower (27 kJ/mol). The observation of lower activation energy could be generated by different reasons. It has been known that the internal diffusion influence could lead to a change in measured activation energy.^{29,30} Although it is not conclusive enough to use values of activation energy alone to explain diffusional influence, the comparable sizes of the pore aperture and cyclohexene make the transport limitation highly possible. The diffusion through the core-shell catalyst is mainly configurational diffusion and the diffusion through the yolk-shell catalyst is a combination of configurational diffusion (shell) and Knudsen diffusion (cavity). This could

1 result in different catalytic behaviors. The other possibility is
2 the kinetics difference due to the conformation of the mole-
3 cules on the metal surface. The size of a cyclohexene mole-
4 cule is about 4.2 Å in its most stable conformation, which is
5 comparable to the size of the aperture (3.4 Å). Thus, the cy-
6 clohexene molecules could only interact with the Pd surface
7 by the successive variation in their conformations in the
8 core-shell structure, in which the ZIF-8 is directly on the Pd
9 surface. It has been shown that the kinetics of six-
10 membered-carbon-ring hydrogenations could be affected by
11 the conformation of the molecules on the metal surface.³¹
12 Detailed studies of the reactions for further understanding
13 the activation energy change are currently under investiga-
14 tion but the study here clearly indicates the importance of
15 the ability to control the cavity for reactions. The ability to
16 create the yolk-shell catalysts provides a strategy to perform
17 selective catalysis without changing the kinetics or generat-
18 ing the diffusional influence.

19 In conclusion, we have developed a general strategy for the
20 synthesis of nanocrystal@ZIF-8 yolk-shell nanostructures.
21 Cu₂O is used as a sacrificial template because it could be
22 etched simultaneously and spontaneously during the forma-
23 tion of ZIF-8. The nanostructures were applied to the gas-
24 phase hydrogenation of ethylene, cyclohexene, and cyclo-
25 octene as catalysts. The ZIF-8 shell shows interesting size-
26 selectivity in ethylene hydrogenation versus cyclohexene
27 hydrogenation. For cyclohexene hydrogenation, the meas-
28 ured activation energy of yolk-shell nanostructure is different
29 from that of the core-shell nanostructure, which demon-
30 strates the influence of the cavity structure in the yolk-shell
31 structures. Integrating the functions of the nanocrystal core,
32 microporous shell, and the cavity in-between provides a new
33 tool to create selective heterogeneous catalysts.

34 SUPPORTING INFORMATION AVAILABLE

35 Detailed experimental procedures, TEM images of Pd Cu-
36 be@ZIF-8, Pt small particle@ZIF-8, and Au octahedron@ZIF-
37 8 yolk-shell structures, XRD patterns, photographs, and TEM
38 images of the samples at different synthetic stages, thermo-
39 gravimetric analysis, and the table of activation energies for
40 cyclohexene hydrogenation. This material is available free of
41 charge via the internet at <http://pubs.acs.org>.

42 ACKNOWLEDGMENT

43 The research is funded by Boston College. Dr. C. H. Kuo
44 thanks National Science Council in Taiwan for offering the
45 scholarship.

46 REFERENCES

- 47 (1) Ikeda, S.; Ishino, S.; Harada, T.; Okamoto, N.; Sakata, T.; Mori, H.;
48 Kuwabata, S.; Torimoto, T.; Matsumura, M. *Angew. Chem. Int. Ed.*
49 **2006**, *45*, 7063.
- 50 (2) Lee, I.; Joo, J. B.; Yin, Y. D.; Zaera, F. *Angew. Chem. Int. Ed.* **2011**,
51 *50*, 10208.
- 52 (3) Zhang, L.; Qiao, S. Z.; Jin, Y. G.; Chen, Z. G.; Gu, H. C.; Lu, G. Q.
53 *Adv. Mater.* **2008**, *20*, 805.
- 54 (4) Gao, J. H.; Liang, G. L.; Cheung, J. S.; Pan, Y.; Kuang, Y.; Zhao, F.;
55 Zhang, B.; Zhang, X. X.; Wu, E. X.; Xu, B. *J. Am. Chem. Soc.* **2008**,
56 *130*, 11828.
- 57 (5) Joo, S. H.; Park, J. Y.; Tsung, C.-K.; Yamada, Y.; Yang, P.; Somor-
58 jai, G. A. *Nat. Mater.* **2009**, *8*, 126.
- 59 (6) Yang, Y.; Liu, J.; Li, X.; Liu, X.; Yang, Q. *Chem. Mater.* **2011**, *23*,
60 3676.

- (7) Lee, J.; Park, J. C.; Song, H. *Adv. Mater.* **2008**, *20*, 1523.
- (8) Liu, J.; Qiao, S. Z.; Hartono, S. B.; Lu, G. Q. *Angew. Chem. Int. Ed.*
2010, *49*, 4981.
- (9) Yin, Y. D.; Rioux, R. M.; Erdonmez, C. K.; Hughes, S.; Somorjai,
G. A.; Alivisatos, A. P. *Science* **2004**, *304*, 711.
- (10) Kuo, C. H.; Huang, M. H. *J. Am. Chem. Soc.* **2008**, *130*, 12815.
- (11) Wu, X. J.; Xu, D. S. *J. Am. Chem. Soc.* **2009**, *131*, 2774.
- (12) Wu, X. J.; Xu, D. S. *Adv. Mater.* **2010**, *22*, 1516.
- (13) Güttel, R.; Paul, M.; Schüth, F. *Catal. Sci. Technol.*, **2011**, *1*, 65.
- (14) Phan, A.; Doonan, C. J.; Uribe-Romo, F. J.; Knobler, C. B.;
O'Keeffe, M.; Yaghi, O. M. *Acc. Chem. Res.* **2010**, *43*, 58.
- (15) Li, K. H.; Olson, D. H.; Seidel, J.; Emge, T. J.; Gong, H. W.; Zeng,
H. P.; Li, J. *J. Am. Chem. Soc.* **2009**, *131*, 10368.
- (16) Venna, S. R.; Carreon, M. A. *J. Am. Chem. Soc.* **2010**, *132*, 76.
- (17) Bux, H.; Feldhoff, A.; Cravillon, J.; Wiebcke, M.; Li, Y. S.; Caro, J.
Chem. Mater. **2011**, *23*, 2262.
- (18) Wu, H.; Zhou, W.; Yildirim, T. *J. Am. Chem. Soc.* **2007**, *129*, 5314.
- (19) Banerjee, R.; Phan, A.; Wang, B.; Knobler, C.; Furukawa, H.;
O'Keeffe, M.; Yaghi, O. M. *Science* **2008**, *319*, 939.
- (20) Jiang, H. L.; Liu, B.; Akita, T.; Haruta, M.; Sakurai, H.; Xu, Q. *J.*
Am. Chem. Soc. **2009**, *131*, 11302.
- (21) Esken, D.; Turner, S.; Lebedev, O. I.; Van Tendeloo, G.; Fischer, R.
A. Chem. Mater. **2010**, *22*, 6393.
- (22) Muller, M.; Hermes, S.; Kaehler, K.; van den Berg, M. W. E.;
Muhler, M.; Fischer, R. A. *Chem. Mater.* **2008**, *20*, 4576.
- (23) Lu, G.; Li, S.; Guo, Z.; Farha, O. K.; Hauser, B. G.; Qi, X.; Wang,
Y.; Wang, X.; Han, S.; Liu, X.; DuChene, J. S.; Zhang, H.; Zhang,
Q.; Chen, X.; Ma, J.; Loo, S. C. J.; Wei, D. W.; Yang, Y.; Hupp, J.
T.; Huo, F. *Nat. Chem.* **2012**, *4*, 310.
- (24) Kuo, C. H.; Hua, T. E.; Huang, M. H. *J. Am. Chem. Soc.* **2009**, *131*,
17871.
- (25) Niu, W. X.; Zhang, L.; Xu, G. B. *ACS Nano* **2010**, *4*, 1987.
- (26) Moh, P. Y.; Cubillas, P.; Anderson, M. W.; Attfield, M. P. *J. Am.*
Chem. Soc. **2011**, *133*, 13304.
- (27) Venna, S. R.; Jasinski, J. B.; Carreon, M. A. *J. Am. Chem. Soc.*
2010, *132*, 18030.
- (28) Fairen-Jimenez, D.; Moggach, S. A.; Wharmby, M. T.; Wright, P.
A.; Parsons, S.; Düren, T. *J. Am. Chem. Soc.* **2011**, *133*, 8900.
- (29) Mears, D. E. *Ind. Eng. Chem. Process Des. Dev.* **1971**, *10*, 541.
- (30) Madon, R. J.; Boudart, M. *Ind. Eng. Chem. Fundam.* **1982**, *21*, 438.
- (31) Bratlje, K. M.; Kliewer, C. J.; Somorjai, G. A. *J. Phys. Chem. B*
2006, *110*, 17925.

